Laminar burning velocity of 2-methylfuran-air mixtures at elevated pressures and temperatures: Experimental and modeling studies

Xu, C., Zhong, A., Wang, H., Jiang, C., Sahu, A., Zhou, W. & Wang, C

Original citation & hyperlink:
Xu, C, Zhong, A, Wang, H, Jiang, C, Sahu, A, Zhou, W & Wang, C 2018, 'Laminar burning velocity of 2-methylfuran-air mixtures at elevated pressures and temperatures: Experimental and modeling studies' Fuel, vol. 231, pp. 215-223. https://dx.doi.org/10.1016/j.fuel.2018.05.082

DOI 10.1016/j.fuel.2018.05.082
ISSN 0016-2361

Publisher: Elsevier

Laminar Burning Velocity of 2-Methlfuran-air Mixtures at Elevated Pressures and Temperatures: Experimental and Modeling Studies

Cangsu Xu[a], Anhao Zhong[a], Hanyu Wang[a], Changzhao Jiang[b], Amrit Sahu[c], Wenhua Zhou[a], Chongming Wang[d*]

[a] *College of Energy Engineering, Zhejiang University, Hangzhou, China, 310027*

[b] *Aeronautical and Automotive Engineering, Loughborough University, Leicestershire, United Kingdom, LE11 3TU*

[c] *Department of Mechanical Engineering, University of Birmingham, Birmingham, United Kingdom, B15 2TT*

[d] *School of Mechanical, Aerospace and Automotive Engineering, Coventry University, Coventry, United Kingdom, CV1 5FB*

[*] Corresponding author e-mail: *ac8174@coventry.ac.uk*

Abstract: 2-Methylfuran (MF), a promising biofuel candidate catalytically produced from biomass-based fructose, has attracted the attention of fuel researchers. However, there is limited data available for the laminar burning velocity, especially at high initial pressure conditions. In this work, the laminar burning velocity of MF-air mixtures at elevated initial pressures (T_0 = 363 K; p_0 = 0.1-0.4 MPa) was experimentally determined in a spherical outwardly expanding flame. Numerical simulation was also conducted in Chemkin using two detailed chemical kinetic mechanisms at elevated pressures (similar to the experiment condition: T_0 = 363 K; p_0 = 0.1-0.4MPa) and elevated temperatures (T_0 = 363-563 K; p_0 = 0.1MPa). Data from experimental and modelling studies were compared and discussed. The experimental results showed that at a given T_0 and p_0 the laminar burning velocity of MF-air mixtures reached peak values at equivalence ratios ϕ = 1.1-1.2, and it slowed down dramatically when the MF-air mixture was too rich or lean. Laminar burning velocity decreased with the increase in p_0. The laminar flame speed of MF-air mixture from two chemical kinetic mechanisms exhibited a similar trend with experimental data; however, both the two mechanisms led to overestimation at the most initial conditions. Compared to the Galway mechanism, the Tianjin mechanism better predicted the laminar burning velocity of MF-air mixtures, especially at initial pressures of 0.1 and 0.2 MPa. The current MF mechanism needs further improvement to better predict the combustion of MF at high-pressure conditions.

Keywords: 2-methylfuran; biofuel; laminar burning velocity; chemical kinetic mechanism

Nomenclature

MF	2-Methylfuran	α	Stretch rate
p_0	Initial pressure	L_b	Markstein length
T_0	Initial temperature	u_L	Laminar burning velocity
A	Area of flame front	ρ_u	Density of unburned gas
t	Time after ignition event	ρ_b	Density of burned gas
R_0	Radius of window	ϕ	Equivalence ratio
r_f	Flame radius	S_b	Stretched flame propagation speed
N	Number of pixels inside the flame front	S_u	Unstretched flame propagation speed
N_{all}	Number of pixels of the entire window		

1. Introduction

Due to the pressures of greenhouse gas emission and limited fossil fuel resources, it is essential to find alternative fuels. Over the past decade, researchers have paid attention to biofuels, such as bioethanol [1, 2], biobutanol [3, 4] and biodiesel [5, 6]. Bioethanol is widely used as a gasoline blending stock because of its renewability, high-octane rating, low carbon footprint and regulation mandatory [7, 8]. However, bioethanol has its limitation, such as low calorific value and water solubility [9].

Román-Leshkov et al. [10] proposed a method of producing furan-based fuel, 2-methylfuran (MF), from biomass-based fructose via acid-catalyzed dehydration and hydrogenolysis processes. The properties of MF are listed in Table 1. Compared to bioethanol and gasoline, MF has several advantages [9]: (1) research octane number (RON) of MF is higher than that of gasoline; (2) the low heating value of MF is much higher than that of bioethanol; (3) unlike ethanol, MF is water-insoluble; (4) the enthalpy of vaporization of MF is lower than that of ethanol, indicating less cold start issues than ethanol.

Table 1: Properties of MF, bioethanol and gasoline [11, 12]

	Gasoline*	Bioethanol	MF
Molecular formula	C_4-C_{12}	C_2H_6O	C_5H_6O
Density @ 20ºC (kg/m^3)	744.6	790.9	913.2
Initial boiling point (ºC)	33	78	64
Research Octane Number	96.8	108	103
Lower heating value (MJ/kg)	42.9	26.8	31.2
Oxygen content (wt.%)	0	34.78	19.51
Enthalpy of vaporization (kJ/kg)	351	919.6	389
Stoichiometric air-fuel ratio (gravimetric)	14.46	8.95	10.05

* Typical main-grade EU gasoline that meets the EN228 regulation

MF has attracted the attention of engine researchers worldwide. Thewes et al. [13] experimentally investigated the influence of MF on spray, evaporation and engine performance in a direct-injection spark-ignition engine. They concluded that MF had quicker vaporisation compared to ethanol, and it had lower hydrocarbon emissions and better knock resistance compared to gasoline. Wang et al. [12] studied the combustion performance and emissions of MF in a direct-injection spark-ignition engine, and they compared the results with those of ethanol and gasoline. The results showed that MF had a better knock suppression ability and a higher indicated thermal efficiency than gasoline had. The particulate emissions from MF were less than gasoline

due to its high oxygen contents. However, NO_x emissions of MF were the highest among the four examined fuels because of its high combustion temperature.

Apart from pure MF, MF-gasoline blends were used as fuels in engines. Wei et al. [14] compared a MF-gasoline blend (M10), ethanol-gasoline (E10) and gasoline in a port-fuel-injection spark ignition engine. With less brake specific fuel consumption, the output torque and brake power of M10 were slightly higher than those of E10. Hydrocarbon and carbon monoxide emissions of M10 were lower than gasoline. Studies go beyond the application of SI engines. Xiao et al. [15] studied combustion performance and emissions of MF-diesel blend fuels in a diesel engine and they concluded that a low MF-diesel blend exhibited a longer ignition delay, a shorter combustion duration and lower soot emissions than pure diesel.

In addition to engine researches, fundamental combustion investigations of MF have been conducted. Somers et al. [16] established a detailed kinetic model of MF oxidation and validated it by experimental ignition delay times and laminar burning velocities. The model highlighted the reactions of the H atom with the fuel. Tran et al. [17] used electron-ionization molecular-beam mass spectrometry and gas chromatography techniques to detect the intermediate species of MF combustion under stoichiometric and fuel-rich premixed low-pressure flames conditions. They developed a detailed kinetic model consisting of 305 species and 1472 reactions. In addition, Cheng et al. [18] analysed the reaction pathway of MF and revised the former MF mechanism under fuel-lean, stoichiometric and fuel-rich conditions. Their mechanism was validated experimentally by detecting the mole fractions of major species in MF flames.

Laminar burning velocity is an important physiochemical parameter of a fuel-air mixture at given temperature and pressure conditions. The knowledge of laminar burning velocity is fundamental to the understanding of other more complicated flame behaviours such as flame extinction, flashback and turbulence combustion. Laminar burning velocity determined in experiments is also used to validate chemical kinetic mechanisms [19]. Laminar burning characteristics of MF and its blends with isooctane have been investigated at the atmospheric pressure, using an outwardly spherical flame method [20, 21]. The results revealed that the laminar burning velocity of MF was faster than that of isooctane.

The laminar burning velocity of MF-air mixtures at high initial pressures is not available in the previous literature. In this work, the laminar burning velocity of MF-air mixtures at elevated initial

pressure (T_0 = 363 K; p_0 = 0.1-0.4 MPa) was experimentally determined with a spherical outwardly expanding flame method. In addition to the experimental study, laminar burning velocity was also simulated by using two chemical kinetic mechanisms at elevated temperatures (T_0 = 363-563 K; p_0 = 0.1MPa) and elevated pressures (T_0 = 363 K; p_0 = 0.1-0.4 MPa). Data from experimental and modelling studies were compared and discussed. In the next section, experimental and numerical methods will be introduced.

2. Experimental and Numerical Methods

2.1 Experimental Setup

Figure 1 presents the experimental setup. The system includes a constant-volume combustion chamber, a Schlieren photography system, an ignition system, an intake and exhaust system, and a data acquisition system.

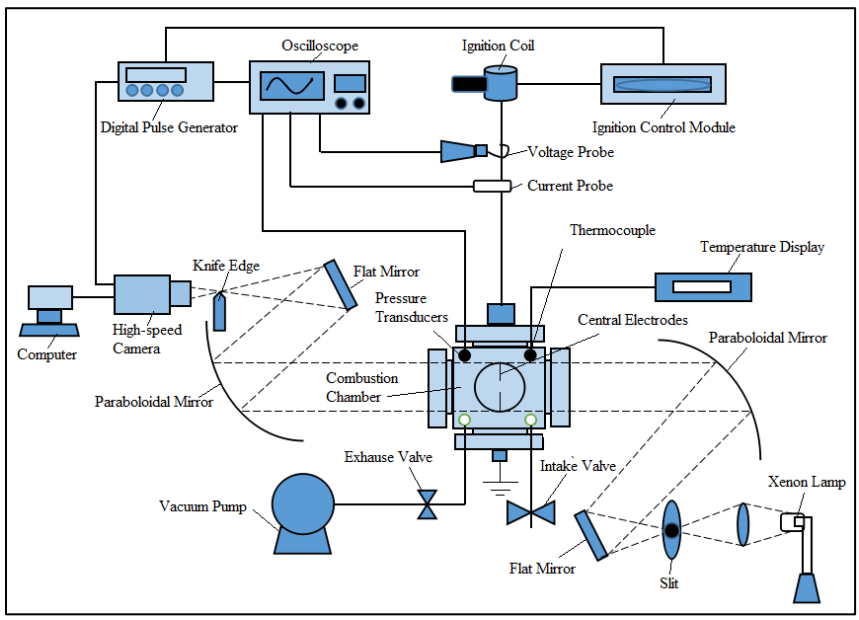

Figure 1: Schematic of the experimental setup

The combustion vessel has a cubical shape, and it is equipped with a pair of quartz windows for the optical access. At each side, there were six cartridge heaters for temperature control. A K-type thermocouple and a pressure gauge were installed to measure the initial mixture temperature and pressure, respectively. Two opposing-electrodes with diameters of 0.4 mm were used for ignition along with an ignition coil and an ignition control module. Flame images were captured by a camera (speed=6000 fps; resolution= 512 × 512). More details about these experimental apparatus and procedures are available in ref. [22, 23].

2.2 Data Processing

In this study, flame fronts of Schlieren images were determined via the Adobe Photoshop software. The radius (r_f) of spherical flame is calculated via:

$$r_f = \sqrt{\frac{N}{N_{all}}} R_W \tag{1}$$

where N, N_{all} and R_W are the pixels inside the flame front, the pixels of the optical window, and the actual radius of the optical window, respectively.

The stretched flame propagation speed (S_b) is calculated via:

$$S_b = \frac{dr_f}{dt} \tag{2}$$

where t is the elapsed time after ignition.

In spherical expanding flames, the stretch rate (α) is defined as [24]：

$$\alpha = \frac{2S_b}{r_f} \tag{3}$$

According to [25], during the quasi-steady period stretched propagation speed and stretch rate have linear relationship:

$$S_b = S_u - L_b\alpha \tag{4}$$

where S_u is the unstretched flame propagation speed; L_b is the Markstein length relative to the burned gas.

With the assumption of a quasi-steady and quasi-planar flame, laminar burning velocity (u_L) is calculated based on the law of mass conservation across the flame front [25]:

$$u_L = \frac{\rho_b}{\rho_u} S_u \tag{5}$$

where ρ_b and ρ_u are the densities of the burned and unburned gas, respectively.

2.3 Experimental Uncertainty Analysis

The primary experiment errors are caused by the uncertainty of initial temperature (ΔU_T), initial pressure (ΔU_p), the number of pixels inside the flame front (ΔU_A), the vessel effective volume (ΔU_V) and the fuel metering (ΔU_F). The accuracy of K-type thermocouples used in this work is $\pm 0.75\%$, and the perturbation of initial temperature can lead to an uncertainty of ~0.8% in the determination

of laminar burning velocity at 0.1 MPa, while at 0.4 MPa the uncertainty can reach ~1.5% [26]. The resolution of the pressure transducer is 0.0001 MPa, and the uncertainty caused by initial pressure is less than 0.1%. In addition, the uncertainty of the pixels inside the flame front is estimated to be ~1%. The uncertainty of the vessel effective volume is ~0.2%. The fuel metering is via a glass syringe with a capacity of 250 μL and with a resolution of 5 μL, and the uncertainty is dependent on the quantity of fuel required for each test condition. In summary, the global laminar burning velocity uncertainty ($\sqrt{\Delta U_T^2 + \Delta U_p^2 + \Delta U_A^2 + \Delta U_V^2 + \Delta U_F^2}$) is within 2% for all the laminar burning velocities tested in this work, and the global equivalent ratio is within 2.5%.

2.4 System Validation

Laminar burning velocity of ethanol-air mixtures were measured at T_0 = 358 K and p_0 = 0.1 MPa. Figure 2 shows the current results and those from Liao et al. [27], Bradley et al. [28] and Laplat et al. [29]. The measurement results in this work are close to those from others; in particular, the average deviation between present results and data reported in Ref. [29] was ~0.01 m/s. This can prove the experimental setup and method in this work are reliable.

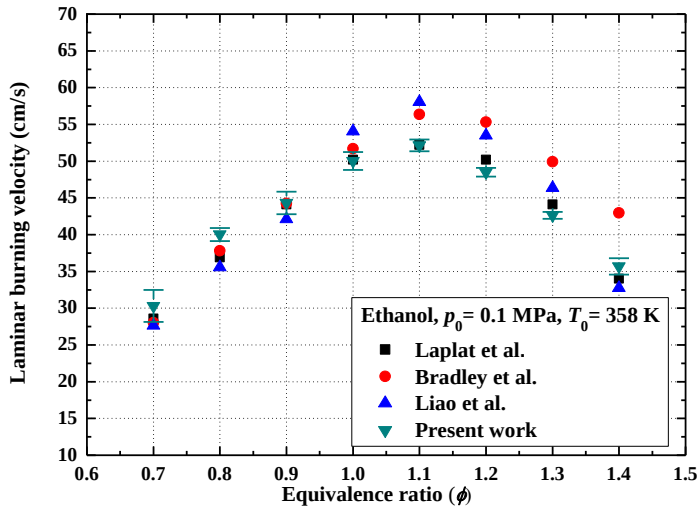

Figure 2: Laminar burning velocities of ethanol-air mixtures measured by the authors' system and presented in the literature (T_0 = 358 K and p_0 = 0.1 MPa)

3. Modelling of Laminar Burning Velocity

Two chemical kinetic mechanisms developed by researchers from Tianjin University (Tianjin Mechanism) [18] and NUI Galway (Galway Mechanism) [16,30-31] were used to simulate the laminar burning velocity of MF-air mixtures in Chemkin.

The Galway mechanism is a detailed chemical kinetic mechanism, consisting of 391 species and 2059 reactions [16,30-31]. This mechanism references several sub-mechanisms from the literature: furan mechanisms [32, 33], aromatic mechanisms [34], H_2 and CO mechanisms [35, 36], light hydrocarbon mechanisms (C_1–C_3) [37, 38], saturated C_4 mechanism [39] and unsaturated C_4 mechanism [40].

The Tianjin mechanism is a detailed chemical kinetic mechanism, consisting of 586 species and 2997 reactions. It is developed based on the Galway Mechanism [30,31]. The Tianjin mechanism updated and emerged some important reactions from Galway Mechanism, such as the reactions related to C_3H_3, benzene, benzyl and fulvene. More fractions of some key species such as MF22J and P134TE1O are quantitively measured to analyse the pathway of MF.

4. Results and Discussion

This section consists of two parts. In the first part, experimental results of the laminar burning velocity for MF-air mixture at elevated initial pressures (T_0 = 363 K, p_0 = 0.1-0.4 MPa) are presented. Before those experimental results are presented, four criteria of flame front radius selection for the determination of laminar burning velocity are discussed. In the second part, results from modelling study using two MF chemical kinetics mechanisms are provided. The modelling study covers the all test condition as the experiments (T_0 = 363 K, p_0 = 0.1-0.4 MPa), and the results from modelling and experiments are compared. In addition, the simulation extends to elevated initial temperatures (T_0 = 363-563 K, p_0 = 0.1MPa).

4.1 Experimental Study

4.1.1 Flame radius selection

There are four criteria for the selection of flame front radius for the determination of laminar burning velocity.

Spark- and wall-affected periods: The development of a spherical outwardly expanding flame in a constant-volume vessel consists of three distinctive periods: an initial period affected by the ignition energy, followed by a quasi-steady period and a final period influenced by the chamber confinement [26]. Laminar flame speed, the value of stretched flame speed extrapolated at zero stretch rate, can be determined from a spherical outwardly expanding flame in a constant-volume

vessel; however, not all the aforementioned stages of flame propagation is suitable for determining the laminar burning velocity. The spark-affected and wall confinement-affected stages need to be identified and be excluded. In this work, flame radii between 8 and 20 mm were used in the determination of laminar burning velocity, which can effectively avoid the spark- and wall-affected periods. Similar flame radii ranges were selected by many research groups [41-43]. It should be noted that the exact range is dependent on the geometry of the vessel and ignition system.

Flame instability and self-acceleration: There is a phenomenon that makes the laminar burning velocity determination difficult at high initial pressure condition in a vessel. At a certain flame propagation stage, flame front becomes unstable, and wrinkle structures appear on the flame surface. The flame front will be accelerated after a critical flame radius, which is the onset point for the unstable flame. If the critical flame radius is too small, the flame radius window suitable for laminar burning velocity calculation will be too small, leading to inaccurate laminar burning velocity. The flame instability can be observed directly from Schlieren images or from the flame propagating speed.

Figure 3 presents the Schlieren flame images of MF-air mixtures at different p_0 and ϕ. p_0 and ϕ had significant impacts on the development of flame morphology. At ϕ = 0.7, the flame surface was smooth at all tested p_0, indicating that the flame was stable. At ϕ = 1.1, the flame surface was smooth at p_0 = 0.1 MPa; however, it developed some cracks/wrinkles, and there were obvious protuberances on the area that in contact with ignition wires at p_0 = 0.2-0.4 MPa, indicating that the flame was unstable. The flame instability was more obvious at ϕ = 1.4, where the clear cellularization was observed at p_0 = 0.2-0.4 MPa. In addition, flame surface cellularization appeared earlier at p_0 = 0.4 MPa than at p_0 = 0.2 MPa. Therefore, the flame instability increased with the increase of p_0 and ϕ.

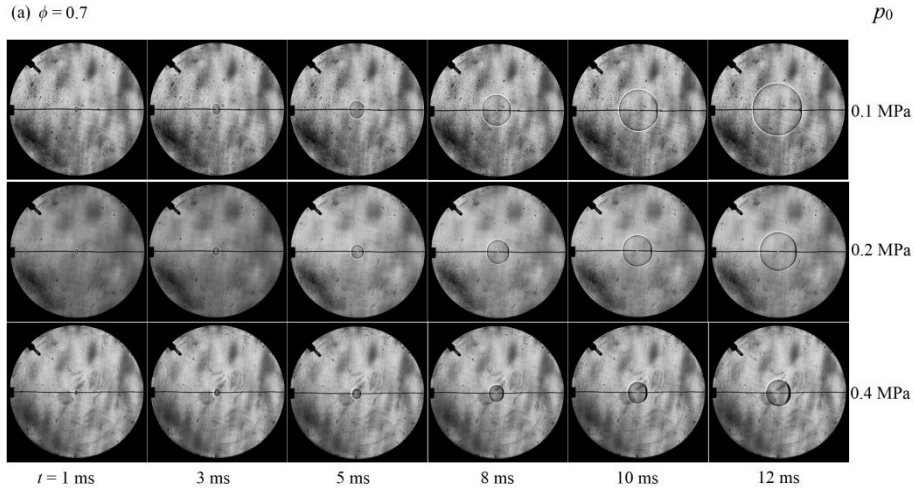

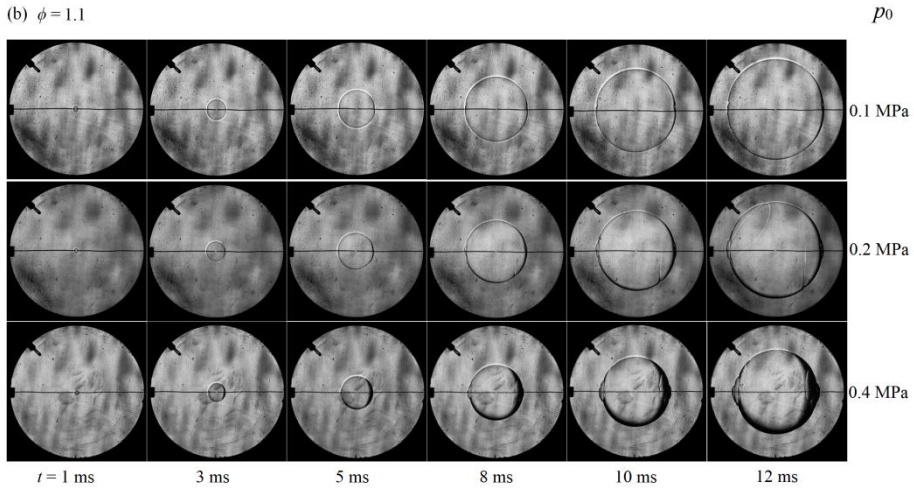

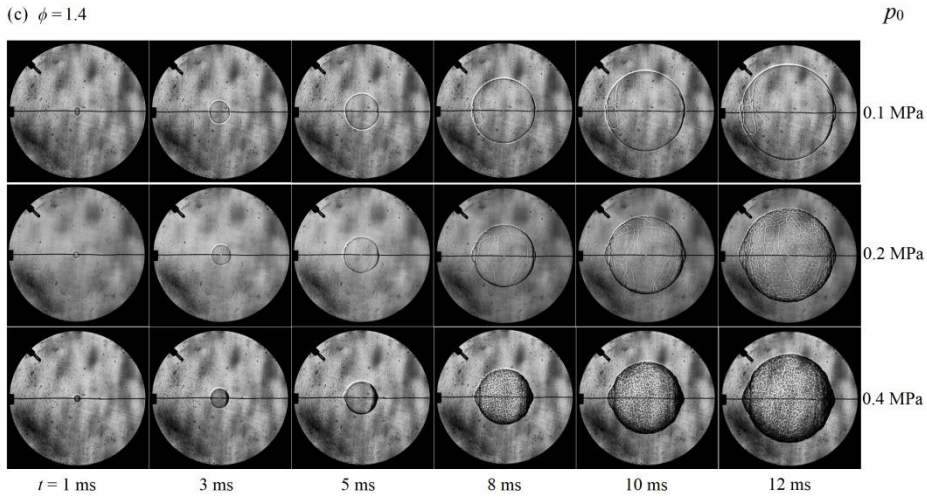

Figure 3: Schlieren images of MF-air mixture flame at T_0 = 363 K, p_0 = 0.1-0.4 MPa: (a) ϕ = 0.7; (b) ϕ = 1.1; and (c) ϕ = 1.4

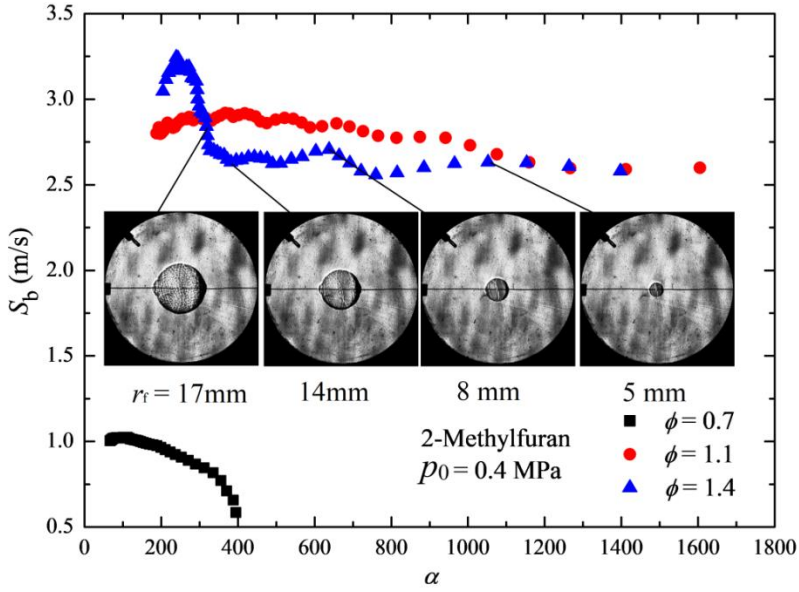

Figure 4: Stretched flame propagation speed versus stretch rate of MF-air mixtures at T_0 = 363 K, p_0 = 0.4 MPa, and ϕ = 0.7, 1.1 and 1.4

Flame surface cellularization may lead to flame self-acceleration. Figure 4 plots stretched flame propagation speed (S_b) versus stretch rate (α) (T_0 = 363 K, p_0 = 0.4 MPa, ϕ = 0.7, 1.1 and 1.4). Some key flame images and flame radius are provided in Figure 4. It can be seen that at ϕ = 1.4, initially, S_b varied little with α, but S_b suddenly increased dramatically at the flame radius of 14 mm. In this study, the determination of laminar burning velocity excluded the flame radius where the flame was unstable or flame self-acceleration was observed.

Pressure: Pressure inside the chamber will increase after the flame develops to a certain size. However, there is an assumption for the use of Equation (2)-(5) to determine the laminar burning velocity: in-vessel pressure must be constant [44]. Figure 5 shows the in-chamber pressure versus time after ignition event of MF-air mixtures at T_0 = 363 K, p_0 = 0.1-0.4 MPa and ϕ = 0.7, 1.1 and 1.4. Flame radius where the pressure started to increase is marked in Figure 5. It is obvious that before the flame radius of 20 mm, no clear in-chamber pressure rise was observed.

Only a small window of flame propagation would be selected for the determination of laminar burning velocity, excluding the effects of ignition energy, chamber wall confinement, flame instability and self-acceleration, and pressure rise. In this work, flame radii between 8 and 20 mm were used for safe determination of laminar burning velocity. For rich MF-air mixtures at 0.4 MPa, the maximum flame radius was decreased to 14 mm due to the cellular structure and self-acceleration.

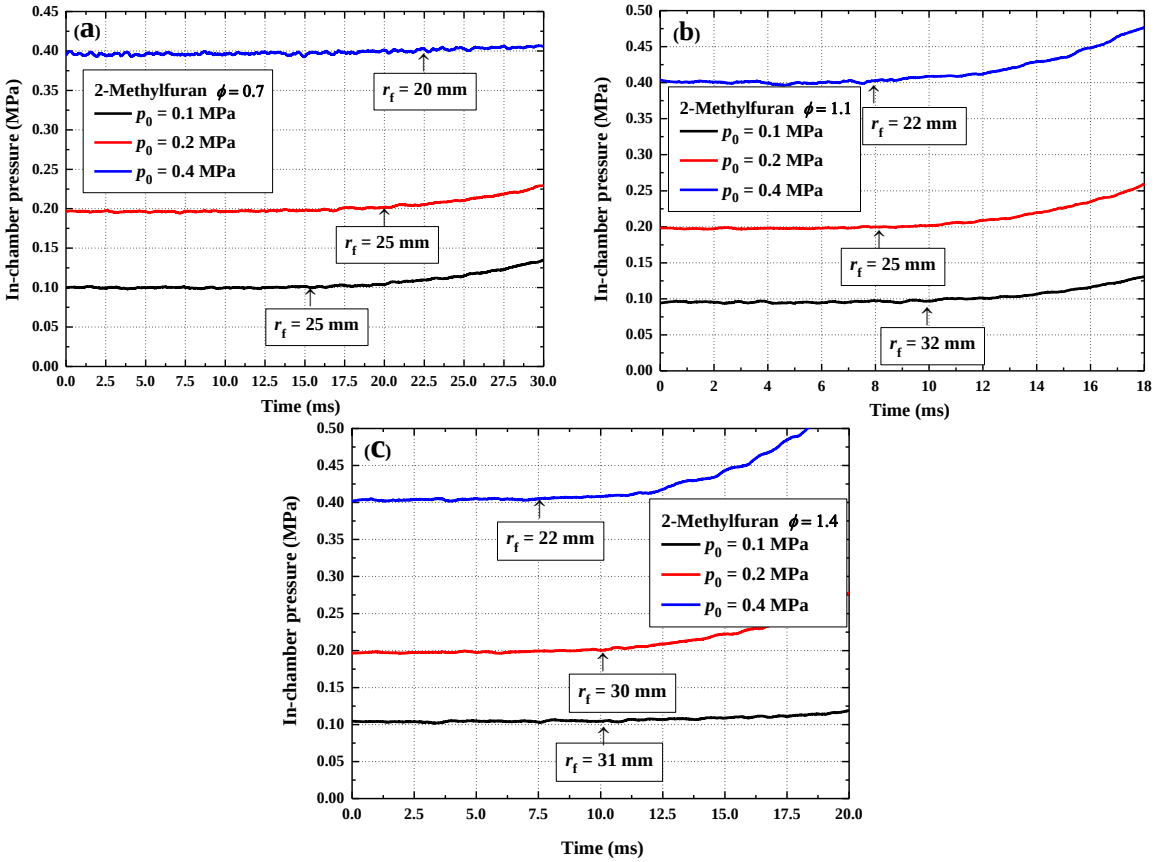

Figure 5: In-chamber pressure versus time after ignition event of MF-air mixtures at T_0 = 363 K and p_0 = 0.1-0.4 MPa: (a) ϕ = 0.7; (b) ϕ = 1.1; and (c) ϕ = 1.4

4.1.2 Laminar burning velocity from experimental study

Figure 6 shows the laminar burning velocity versus ϕ at T_0 = 363 K and p_0 = 0.1-0.4 MPa. As p_0 increased, laminar burning velocity decreased, due to the increased rates of the three-body recombination reactions [45]. This trend is consistent with the results of other fuels, such as ethanol [28] and DMF [45]. Within the range of ϕ = 0.7-1.1, the laminar burning velocity at p_0 = 0.1 MPa was averagely 16.6% and 37.5% faster than that at p_0 = 0.2 MPa and p_0 = 0.4 MPa, respectively. The peak value of laminar burning velocity was occurred at ϕ = 1.1 at p_0 = 0.1 and 0.2 MPa, and at ϕ = 1.2 at p_0 = 0.4 MPa.

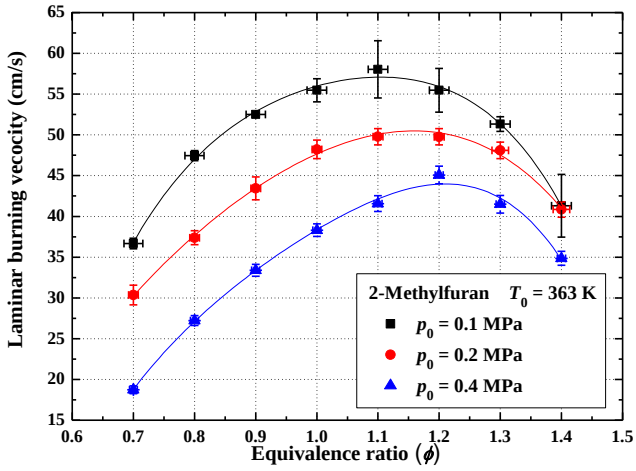

Figure 6: Laminar burning velocity of MF-air mixtures at T_0 = 363 K and p_0 = 0.1-0.4 MPa

4.2 Modeling Simulation

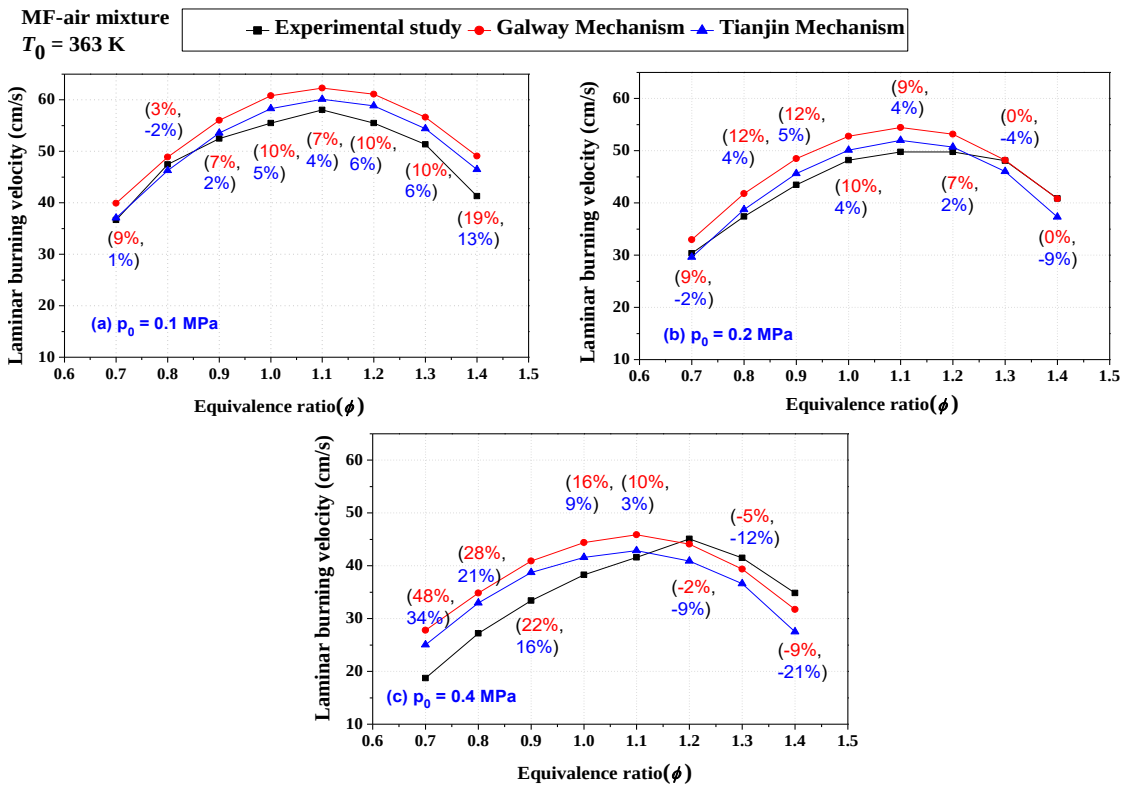

Figure 7: Comparison of experimental and simulated laminar burning velocity of MF-air mixtures at T_0 =363 K and p_0 = 0.1-0.4 MPa

Figure 7 shows the laminar burning velocities of MF-air mixtures at T_0 = 363 K and p_0 = 0.1-0.4 MPa, simulated in two chemical kinetic mechanisms developed by researchers from Tianjin University (Tianjin Mechanism) and NUI Galway (Galway Mechanism), and the simulation results

are compared with experimental data in this research. Results from both mechanisms show that laminar burning velocity reached the maximum value at given initial T_0 and p_0 at approximately ϕ = 1.1, and the laminar burning velocity profile was symmetric with respect to ϕ = 1.1. This finding is similar to the experimental results shown in Figure 6. There are two numbers in the bracket near each data point in Figure 7: the top number means the percentage difference between results from experiments and Galway mechanism; the bottom number means the percentage difference between results from experiments and Tianjin mechanism. It can be seen that both Galway and Tianjin mechanisms overestimated laminar burning velocities of MF-air mixtures at most conditions, apart from for rich mixtures (p_0 = 0.2 and 0.4 MPa) where both mechanisms gave underestimated laminar burning velocities. Comparing two mechanisms, the results from Tianjin mechanism was closer to the experimental results, especially at the initial pressure of 0.1 and 0.2 MPa (the percentage difference was mostly less than 6%). Because the authors of Tianjin mechanism measured the mole fractions of several important intermediate products (MF22J, P134TE1O, etc.), and analysed the reaction pathways of MF combining the Galway mechanism and their experimental data. However, the discrepancy became larger for lean and rich conditions (the percentage difference was more than 20%) at the initial pressure of 0.4 MPa. The mechanism needs further modification to be used for high-pressure simulation.

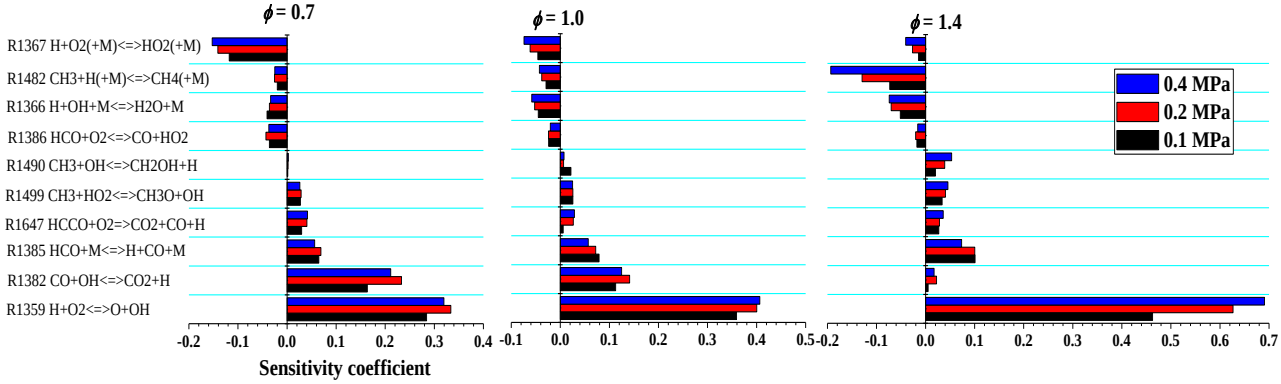

Figure 8: Sensitivity analyses of MF-air flames using Tianjin mechanism at three different equivalence ratios (0.7, 1.0 and 1.4) and three initial pressures (0.1, 0.2 and 0.4 MPa)

Figure 8 shows the sensitivity analyses of MF-air flame at different equivalence ratios and different initial pressures. The sensitivity analyses were conducted for the Tianjin mechanism. The influence of rate constant of each reaction on the flame speed was reflected by the sensitivity coefficient. The most important reaction was R1359, which increased the number of active radicals

in flame; and its sensitivity coefficient was increased with the increase of equivalence ratio and initial pressure, except for the situation from 0.2 to 0.4 MPa at ϕ = 0.7. For lean and stoichiometric conditions, the oxidation of CO to CO_2 by OH (R1382) had a significant positive effect on flame speed, and the sensitivity coefficient was decreased with the increase of equivalence ratio. The decomposition of HCO (R1385) increased the flame speed to some extent. In addition, the flame speed was slightly promoted by R1499 and R1647 for all the initial conditions; and for rich conditions, the flame speed could also be increased by R1490. There exists some reactions with negative sensitivity coefficient which inhibit the flame speed. Reactions had large inhibiting effect were three-body reactions, such as the combinations of H and O_2 (R1367), CH_3 and H (R1482), and H and OH (R1366), etc. The sensitivity coefficients of them were decreased with the increase of initial pressure. Since the three-body reactions are the key reactions in reproducing the experiments at higher initial pressure. Therefore, the three-body reactions should be further modified to better reproduce the experiment at higher pressures.

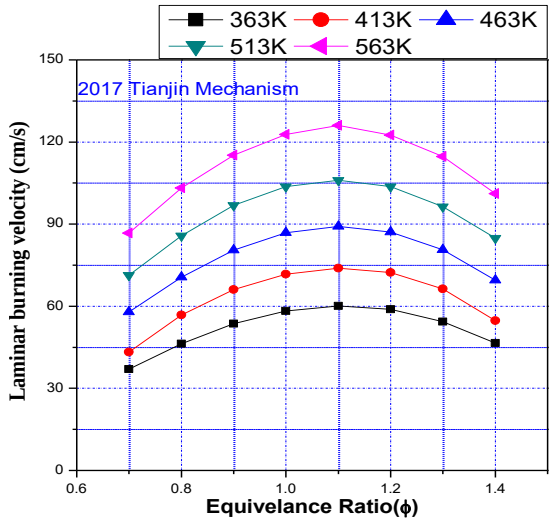

Figure 9: Simulated laminar burning velocity of MF-air mixtures at T_0 = 363-563 K and p_0 = 0.1MPa (Tianjin Mechanism)

The simulation is extended to conditions beyond the experimental conditions. Figure 9 shows the laminar burning velocity of MF-air mixtures at T_0 = 363-563 K and p_0 = 0.1MPa, simulated by the Tianjin Mechanism. Again, the laminar burning velocity trend with respect to ϕ is highly similar to the results shown in Figure 7. At a given equivalence ratio, the laminar burning velocity increases with T_0, and the increase rate is positive. This was caused by the enhanced chemical reaction rate at a higher temperature.

5. Conclusions

In this work, an experimental study of the laminar burning velocity of MF-air mixtures at elevated initial pressure (T_0 = 363 K; p_0 = 0.1-0.4 MPa) was conducted in the spherical outwardly expanding flame. Laminar burning velocity was also simulated in Chemkin using two chemical kinetic mechanisms at elevated initial temperatures (T_0 = 363-563 K; p_0 = 0.1MPa) and elevated initial pressures (T_0 = 363 K; p_0 = 0.1-0.4 MPa). Experiments show that the laminar burning velocity of MF-air mixtures was firstly increased and then decreased as the ϕ increased from 0.7 to 1.4. At given p_0 and T_0, the maximum values of laminar burning velocities were observed at ϕ = 1.1-1.2. p_0 had a negative influence on the laminar burning velocity. Simulation results showed a similar trend with experimental results; however, both the Tianjin and Galway mechanisms overestimated the laminar burning velocity of MF-air mixtures at most initial conditions, apart from for rich mixtures (p_0 = 0.2 and 0.4 MPa) where both mechanisms gave underestimated laminar burning velocities. Compared to the Galway mechanism, the Tianjin mechanism consistently produced a more accurate prediction of the laminar burning velocity of MF-air mixtures. At the initial pressures of 0.1 and 0.2 MPa, the percentage difference was almost less than 6%; however, at higher initial pressure (p_0 = 0.4 MPa), the discrepancy between experimental and simulation results became larger at lean and rich conditions (discrepancy > 20%). This shows that the current MF mechanism requires some revision for a better prediction of laminar flame speed at high initial pressure.

Acknowledgements

This work was financially supported by the Engineering and Physical Sciences Research Council (NO. EP/N021746/1), the Public Beneficial Technology Application Research Project of the Science Technology Department of Zhejiang Province (No. 2016C31102), and National Basic Research Program (No. 2013CB228106) of China.

Reference

[1] C. Wang, A. Prakash, A. Aradi, R. Cracknell, H. Xu, Significance of RON and MON to a modern DISI engine, Fuel, 209 (2017) 172-183.

[2] C. Wang, A. Janssen, A. Prakash, R. Cracknell, H. Xu, Splash blended ethanol in a spark ignition engine – Effect of RON, octane sensitivity and charge cooling, Fuel, 196 (2017) 21-31.

[3] Y. Wang, S.H. Ho, H.W. Yen, D. Nagarajan, N.Q. Ren, S. Li, Z. Hu, D.J. Lee, A. Kondo, J.S. Chang, Current advances on fermentative biobutanol production using third generation feedstock, Biotechnology advances, (2017).

[4] M.F. Ibrahim, N. Ramli, E. Kamal Bahrin, S. Abd-Aziz, Cellulosic biobutanol by Clostridia: Challenges and improvements, Renewable and Sustainable Energy Reviews, 79 (2017) 1241-1254.

[5] E. Buyukkaya, Effects of biodiesel on a DI diesel engine performance, emission and combustion characteristics, Fuel, 89 (2010) 3099-3105.

[6] J. Xue, T.E. Grift, A.C. Hansen, Effect of biodiesel on engine performances and emissions, Renewable and Sustainable Energy Reviews, 15 (2011) 1098-1116.

[7] C. Wang, S. Zeraati-Rezaei, L. Xiang, H. Xu, Ethanol blends in spark ignition engines: RON, octane-added value, cooling effect, compression ratio, and potential engine efficiency gain, Applied Energy, 191 (2017) 603-619.

[8] H. Xu, C. Wang, X. Ma, A.K. Sarangi, A. Weall, J. Krueger-Venus, Fuel injector deposits in direct-injection spark-ignition engines, Progress in Energy and Combustion Science, 50 (2015) 63-80.

[9] C.M. Wang, H.M. Xu, R. Daniel, A. Ghafourian, J.M. Herreros, S.J. Shuai, X. Ma, Combustion characteristics and emissions of 2-methylfuran compared to 2,5-dimethylfuran, gasoline and ethanol in a DISI engine, Fuel, 103 (2013) 200-211.

[10] Y. Roman-Leshkov, C.J. Barrett, Z.Y. Liu, J.A. Dumesic, Production of dimethylfuran for liquid fuels from biomass-derived carbohydrates, Nature, 447 (2007) 982-985.

[11] H. Wei, D. Gao, L. Zhou, D. Feng, C. Chen, Z. Pei, Experimental analysis on spray development of 2-methylfuran–gasoline blends using multi-hole DI injector, Fuel, 164 (2016) 245-253.

[12] C. Wang, H. Xu, R. Daniel, A. Ghafourian, J.M. Herreros, S. Shuai, X. Ma, Combustion characteristics and emissions of 2-methylfuran compared to 2,5-dimethylfuran, gasoline and ethanol in a DISI engine, Fuel, 103 (2013) 200-211.

[13] M. Thewes, M. Muether, S. Pischinger, M. Budde, A. Brunn, A. Sehr, P. Adomeit, J. Klankermayer, Analysis of the Impact of 2-Methylfuran on Mixture Formation and Combustion in a Direct-Injection Spark-Ignition Engine, Energy & Fuels, 25 (2011) 5549-5561.

[14] H. Wei, D. Feng, G. Shu, M. Pan, Y. Guo, D. Gao, W. Li, Experimental investigation on the combustion and emissions characteristics of 2-methylfuran gasoline blend fuel in spark-ignition engine, Applied Energy, 132 (2014) 317-324.

[15] H. Xiao, P. Zeng, Z. Li, L. Zhao, X. Fu, Combustion performance and emissions of 2-methylfuran diesel blends in a diesel engine, Fuel, 175 (2016) 157-163.

[16] K.P. Somers, J.M. Simmie, F. Gillespie, U. Burke, J. Connolly, W.K. Metcalfe, F. Battin-Leclerc, P. Dirrenberger, O. Herbinet, P.A. Glaude, H.J. Curran, A high temperature and atmospheric pressure experimental and detailed chemical kinetic modelling study of 2-methyl furan oxidation, Proceedings of the Combustion Institute, 34 (2013) 225-232.

[17] L.S. Tran, C. Togbe, D. Liu, D. Felsmann, P. Osswald, P.A. Glaude, R. Fournet, B. Sirjean, F. Battin-Leclerc, K. Kohse-Hoinghaus, Combustion chemistry and flame structure of furan group

biofuels using molecular-beam mass spectrometry and gas chromatography - Part II: 2-Methylfuran, Combust and Flame, 161 (2014) 766-779.
[18] Z. Cheng, Q. Niu, Z. Wang, H. Jin, G. Chen, M. Yao, L. Wei, Experimental and kinetic modeling studies of low-pressure premixed laminar 2-methylfuran flames, Proceedings of the Combustion Institute, 36 (2017) 1295-1302.
[19] X. Bao, Y. Jiang, H. Xu, C. Wang, T. Lattimore, L. Tang, Laminar flame characteristics of cyclopentanone at elevated temperatures, Applied Energy, 195 (2017) 671-680.
[20] X. Ma, C. Jiang, H. Xu, S. Shuai, H. Ding, Laminar Burning Characteristics of 2-Methylfuran Compared with 2,5-Dimethylfuran and Isooctane, Energy & Fuels, 27 (2013) 6212-6221.
[21] X. Ma, C. Jiang, H. Xu, H. Ding, S. Shuai, Laminar burning characteristics of 2-methylfuran and isooctane blend fuels, Fuel, 116 (2014) 281-291.
[22] C. Xu, D. Fang, Q. Luo, J. Ma, Y. Xie, A comparative study of laser ignition and spark ignition with gasoline–air mixtures, Optics & Laser Technology, 64 (2014) 343-351.
[23] C. Xu, Y. Hu, X. Li, X. Zhou, A. Zhong, Comparative experimental study of ethanol-air premixed laminar combustion characteristics by laser induced spark and electric spark ignition, Korean Journal of Chemical Engineering, 34 (2017) 574-579.
[24] Y. Di, Z. Huang, N. Zhang, B. Zheng, X. Wu, Z. Zhang, Measurement of Laminar Burning Velocities and Markstein Lengths for Diethyl Ether-Air Mixtures at Different Initial Pressure and Temperature, Energy & Fuels, 23 (2009) 2490-2497.
[25] D. BRADLEY, R.A. HICKS, M. LAWES, C.G.W. SHEPPARD, R. WOOLLEY, The Measurement of Laminar Burning Velocities and Markstein Numbers for Iso-octane-Air and Iso-octane-n-Heptane-Air Mixtures at Elevated Temperatures and Pressures in an Explosion Bomb, Combustion and Flame, 115 (1998) 126-144.
[26] Z. Chen, On the accuracy of laminar flame speeds measured from outwardly propagating spherical flames: Methane/air at normal temperature and pressure, Combustion and Flame, 162 (2015) 2442-2453.
[27] S.Y. Liao, D.M. Jiang, Z.H. Huang, K. Zeng, Q. Cheng, Determination of the laminar burning velocities for mixtures of ethanol and air at elevated temperatures, Applied Thermal Engineering, 27 (2007) 374-380.
[28] D. Bradley, M. Lawes, M.S. Mansour, Explosion bomb measurements of ethanol–air laminar gaseous flame characteristics at pressures up to 1.4MPa, Combustion and Flame, 156 (2009) 1462-1470.
[29] N. Leplat, P. Dagaut, C. Togbé, J. Vandooren, Numerical and experimental study of ethanol combustion and oxidation in laminar premixed flames and in jet-stirred reactor, Combustion and Flame, 158 (2011) 705-725.
[30] K.P. Somers, J.M. Simmie, W.K. Metcalfe, H.J. Curran, The pyrolysis of 2-methylfuran: a quantum chemical, statistical rate theory and kinetic modelling study, Physical Chemistry Chemical Physics, 16 (2014) 5349-5367.
[31] K.P. Somers, J.M. Simmie, F. Gillespie, C. Conroy, G. Black, W.K. Metcalfe, F. Battin-Leclerc, P. Dirrenberger, O. Herbinet, P.-A. Glaude, P. Dagaut, C. Togbé, K. Yasunaga, R.X. Fernandes, C. Lee, R. Tripathi, H.J. Curran, A comprehensive experimental and detailed chemical kinetic modelling study of 2,5-dimethylfuran pyrolysis and oxidation, Combustion and Flame, 160 (2013) 2291-2318.
[32] K. Sendt, G.B. Bacskay, J.C. Mackie, Pyrolysis of furan: Ab initio quantum chemical and kinetic modeling studies, The Journal of Physical Chemistry A, 104 (2000) 1861-1875.

[33] Z. Tian, T. Yuan, R. Fournet, P.-A. Glaude, B. Sirjean, F. Battin-Leclerc, K. Zhang, F. Qi, An experimental and kinetic investigation of premixed furan/oxygen/argon flames, Combustion and Flame, 158 (2011) 756-773.
[34] W. Metcalfe, S. Dooley, F. Dryer, Comprehensive detailed chemical kinetic modeling study of toluene oxidation, Energy & Fuels, 25 (2011) 4915-4936.
[35] A. Kéromnes, W. Metcalfe, N. Donohoe, H. Curran, W. Pitz, Detailed chemical kinetic model for H2 and H2/CO (syngas) mixtures at elevated pressure, in, Lawrence Livermore National Laboratory (LLNL), Livermore, CA, 2011.
[36] A. Kéromnès, W.K. Metcalfe, K.A. Heufer, N. Donohoe, A.K. Das, C.-J. Sung, J. Herzler, C. Naumann, P. Griebel, O. Mathieu, An experimental and detailed chemical kinetic modeling study of hydrogen and syngas mixture oxidation at elevated pressures, Combustion and Flame, 160 (2013) 995-1011.
[37] W. Lowry, J. de Vries, M. Krejci, E. Petersen, Z. Serinyel, W. Metcalfe, H. Curran, G. Bourque, Laminar flame speed measurements and modeling of pure alkanes and alkane blends at elevated pressures, Journal of Engineering for Gas Turbines and Power, 133 (2011) 091501.
[38] W.K. Metcalfe, S.M. Burke, C.K. Aul, E.L. Petersen, H.J. Curran, A Detailed Chemical Kinetic Modelling and Experimental Study of C1–C2 Hydrocarbons, Proceedings of the European Combustion Meeting, Cardiff, (2011).
[39] D. Healy, N. Donato, C. Aul, E. Petersen, C. Zinner, G. Bourque, H. Curran, n-Butane: Ignition delay measurements at high pressure and detailed chemical kinetic simulations, Combustion and Flame, 157 (2010) 1526-1539.
[40] A. Laskin, H. Wang, C.K. Law, Detailed kinetic modeling of 1, 3-butadiene oxidation at high temperatures, International Journal of Chemical Kinetics, 32 (2000) 589-614.
[41] C. Xu, A. Zhong, X. Li, C. Wang, A. Sahu, H. Xu, T. Lattimore, K. Zhou, Y. Huang, Laminar burning characteristics of upgraded biomass pyrolysis fuel derived from rice husk at elevated pressures and temperatures, Fuel, 210 (2017) 249-261.
[42] E. Hu, Z. Huang, J. He, H. Miao, Experimental and numerical study on laminar burning velocities and flame instabilities of hydrogen–air mixtures at elevated pressures and temperatures, International Journal of Hydrogen Energy, 34 (2009) 8741-8755.
[43] A. Kelley, C. Law, Nonlinear effects in the extraction of laminar flame speeds from expanding spherical flames, Combustion and Flame, 156 (2009) 1844-1851.
[44] M. Faghih, Z. Chen, The constant-volume propagating spherical flame method for laminar flame speed measurement, Science Bulletin, 61 (2016) 1296-1310.
[45] X. Wu, Z. Huang, X. Wang, C. Jin, C. Tang, L. Wei, C.K. Law, Laminar burning velocities and flame instabilities of 2,5-dimethylfuran–air mixtures at elevated pressures, Combustion and Flame, 158 (2011) 539-546.